# Creating High Yield Stress Particle Laden Oil/Water Interfaces using Charge Bidispersity

**Authors:** Arsalan Abutalebi[1] and Gordon F. Christopher[1*]

[1]Department of Mechanical Engineering, Whitacre College of Engineering, Texas Tech University, Lubbock TX

*corresponding author: Gordon.christopher@ttu.edu

## Abstract

There has been increasing use of interfacial engineering to stabilize Pickering emulsions in commercial products and biomedical applications. Pickering emulsion stabilization is aided by interfacial viscoelasticity, but typically the primary means of stabilization are steric hinderances between high surface concentration shells of particles around drops. In this work, the concept of creating large interfacial viscoelastic yield stresses with low particle surface concentrations (<50%) using bidisperse charged particle systems is tested to evaluate their potential efficacy in emulsion stabilization. To explore this hypothesis, interfacial rheology and visualization experiments are conducted at o/w interfaces using positively charged amidine, negatively charged carboxylate, and negatively charged sulfate coated latex spheres and compared to a model based on interparticle forces. Bidisperse particle systems are observed to create more networked structures in comparison to monodisperse systems. For surface concentrations <50%, bidisperse interfaces created measurable viscoelastic moduli ~1 order of magnitude larger than monodisperse interfaces. Furthermore, these interfaces had measurable yield stresses on the order of $10^{-4}$ Pa*m when monodisperse systems had none. Bidispersity impacts surface viscoelasticity primarily due to increasing the overall magnitude of attraction between particles at the interface, and not due to changes in microstructure. The developed model predicts what relative surface fraction creates the largest moduli and shows good agreement to experimental data. The results show the ability to create large viscoelastic moduli for small surface fractions of particles, which may enable stabilization using fewer particles in future applications.

**Key Words:** Interfacial Rheology, Pickering Emulsions, Particle Laden Interfaces

## Introduction

Fluid/fluid interfacial engineering has gained significant attention as it plays a central role in stabilizing a wide range of commercial and industrial foams and emulsions. Although there are a range of surface active materials for such interfacial engineering, colloidal particles have found increasing use to stabilize emulsions across a range of applications, including enhanced oil recovery,[1-2] food,[3-5] polymer engineering,[6] 3D printing,[7] environmental remediation,[8] antimicrobial treatments,[9] and cosmetic formulations.[10] Colloids irreversibly adsorb to an interface, hindering droplet coalescence, forming a stable Pickering emulsion.[11] The surface properties of the particles themselves dictate the properties and type of Pickering emulsion,[12] in particular wettability and charge have significant impact.[13-15]

Typically, the assumption is that the stabilization mechanism of particles around droplets in Pickering emulsions has been due to their near full coverage creating an "armor" like shell.[16] Such assumptions have also been held for particle stabilized foams.[17] However, recent work has shown that that well engineered particle laden air/water interfaces with sufficient interfacial yield stress are more than capable of resisting dissolution and Ostwald ripening of particle stabilized foams when under compressive pressure loading. The results show that the key parameter limiting the dissolution is interfacial yield stress. Even lower surface coverage interfaces made with ellipsoidal particles can create stable foams due to their ability to create larger yield stresses at low surface concentrations.[18] Such result have led to the hypothesis that stable foams could be made from low surface concentration interfaces engineered using particle size, shape, and surface chemistry to modify interparticle forces to create sufficient interfacial yield.[19]

In this work, the goal is to explore whether such high interfacial yield stress, low surface concentration particle surfaces are possible at o/w interfaces, where interfacial forces typically work against their formation. To understand why it may be more difficult to engineer lower surface concentration, high yield o/w interfaces, it is necessary to understand the fundamental forces that control particle behavior at o/w interfaces and what is already known about the mechanics of particle laden interfaces, focusing on the behavior of hard spheres microparticles. There are three primary interactions that occur between such particles at o/w or a/w interfaces.

The first force is the electrostatic interaction between charged particles; due to being trapped at the interface, the particles develop charge distribution within the Debye length in the aqueous phase and no charge within the non-polar oil, resulting in the formation of electrostatic dipoles through the particles, creating strong, long-range interactions. Depending on relative dipole alignment, these interactions can be either attractive or repulsive.[20] Because this force occurs across the interface, it is highly dependent on the dielectric constant of the interfaces.[21] The electric field created by the dipole that causes the force, can either be transmitted due to charges trapped at the particle/non-polar interface or through the polar phase.[22] Importantly, if the force is carried through the polar phase, it is explicitly tied to the Debye layer of the particle, and hence the ionic concentration of the polar phase.[22]

The second primary force between interfacial particles is a capillary force. Unlike larger particles, capillary forces between colloids occur due to interfacial deformation caused by contact line undulation.[23] The resulting interface deformation is complicated, but in literature has been found to best modeled as a quadrupole.[23-24] Interestingly, this deformation results in an angular dependence of the capillary force where aligned particles will have attractive interactions and unaligned particles will have repulsive forces

with torques attempting to create alignment. [24-25] Due to the nature of the force, the magnitude and strength are highly dependent on the particle shape,[26] roughness,[27]wettability,[28] hardness,[29] charge,[30] and the presence of other adsorbed materials.[31-32]

Finally, hydrophobic particles at interfaces also exhibit a typically large attractive force known as a hydrophobic attraction. This force arises due to the physical phenomenon of hydrophobic surfaces minimizing contact between themselves and water surfaces, and its overall magnitude is dependent on specific system composition.[33] Importantly, it can lead to strong differences in interfacial viscoelastic moduli between hydrophilic and hydrophobic particles, due to increased attraction of hydrophobic particles.[34]

There have been several studies examining how changes to subphase/interface composition impact the relative effects on these forces to create stronger interfaces from monodisperse particle populations. For instance, overall salt concentration has been found to reduce the magnitude of electrostatic interactions, resulting in aggregation and greater viscoelastic moduli in measurement.[35-37] Furthermore, the subphase composition will also impact electrostatic forces, with o/w interface exhibiting larger repulsions in comparison to a/w systems due to the difference in dielectric constants, as previously mentioned.[20] Because of the change in contact angles and decrease in contact line undulation, a/w interfaces exhibit a more monopolar capillary charge in comparison to the quadrupole charge of o/w interfaces, allowing less repositioning of particles at a/w interfaces and stronger capillary bonds between particles.[38-39] In general, literature indicates increasing ionic concentration of polar subphases will create larger viscoelastic moduli and a/w interfaces typically have larger moduli than o/w due to increases in capillary bond rigidity and reduction of dipole repulsion.

Additionally, for monodisperse particle populations properties such as particle size[40], shape,[18] charge,[41] roughness,[42-43], deformability,[44] and wettability[45] have been observed to impact both microstructure and mechanical properties of these interfaces by influencing capillarity and/or electrostatic repulsions. In order to provide even greater opportunity for controlling the mechanical properties and rheology of these interfaces, many studies have looked at using Janus particles which has recently been well reviewed[46] and are found to form highly elastic and more networked like structures due to their amphiphilicity.

In the above studies, one commonality is the use of monodisperse particle systems. Even in the case of more complicated Janus particle systems, the particles are all a single type. The resulting systems can have large viscoelastic moduli, but usually only at large surface concentrations with increasingly small moduli at lower surface concentrations. However, many studies of Pickering emulsions' bulk behavior have shown that controlled particle bidispersity in charge, size, wettability, and hardness all improve bulk emulsion stability; these studies are well covered in the recent revie article of Liu and Ngai.[47] This indicates bidispersity is enhancing the mechanical properties of drops and hence their interfaces. This may be an avenue to decrease surface concentration while still creating large interfacial yield stresses.

A few studies have examined controlled bidispersity as a means of engineering an interface. Qiao and coworkers showed adding small fraction of Janus particles to the interface results in the formation of clusters around the Janus particles, creating a more elastic and higher modulus interface.[48] Ballard and coworkers found that size bidispersity on spherical interfaces allows smaller particles to fix defects in an overall crystal packing structure.[49] Monteaux and coworkers showed that bidisperse sized particles with

identical charge on spherical interfaces create systems with areas of identical particles and compressible holes at grain boundaries.[50] On a flat interface, Nallamilli and coworkers have shown that charge bidisperse particles create long range, percolated networks when near equivalent relative concentrations of particle.[41] Bidisperse wettability particles increase microstructure connectivity similar to bidispersity in charge,and relative elasticity on a/w interfaces, which was theorized to be due to relative probability of particle interactions with opposite type particles.[51]

Given previous results on bulk emulsions and bidisperse interfaces, bidispersity at an o/w interface may create a low surface concentration, high yield stress interface capable of stabilizing an emulsion. However, there are still unanswered questions regarding this topic. Bidisperse emulsion studies use high particle volume fractions, which create high surface coverage droplets that are primarily protected due to the armor like effect. Furthermore, there is little understanding how and why bidispersity increases moduli, making designing systems impossible. In this paper, o/w interfaces with polystyrene particles of opposite charge are characterized experimentally and used to create high interfacial stress, low surface concentration interfaces. A model is developed to predict the relative surface concentration of maximum impact.

## Materials and Method

### *Particles*

Three types of particle types were used to create interfaces. The first were a positively charged Amidine particles (Thermo Fisher Scientific, Lot No. 2530683) with a mean diameter of 0.98μm and a surface charge density of 25.4 μC/cm². The second were negatively charged sulfate particles (Thermo Fisher Scientific, Lot No. 1071785) with a mean diameter of 0.99 μm and a surface charge density of 5.3 μC/cm². Finally, negatively charged Carboxylate particles (Polysciences Inc., Lot No. 695542) with a reported mean diameter of 1μm were used. For **these** particles, a surface charge density of 8.47 μC/cm² was calculated experimentally using a zetaziser (Microtrac) and assuming a small Debye length.[52]

Particles were cleaned of surfactant and impurities by centrifuging for 60 min at 4400rpm (Eppendorf 5702), removing supernatant and replacing with fresh DI water of equal volume; this process was repeated 10 times. Stock particle solutions were made from cleaned particles by combining predetermined volumes of cleaned particle solution with DI water.

### *Interface composition*

Aqueous subphase contained 70% by volume DI water and 30% by volume Glycerol to prevent particle sedimentation. The oil supra phase was composed of silicone oil (Sigma Aldrich) with 10cSt viscosity at 25 °C was used. Particle systems are identified by αXXβYY to identify both particle composition: where A stands for Amidine, C for Carboxylate and S for Sulfate when replacing α,β and XX/YY are the percentage of each respective preceding particle.

Interfaces were created by spreading a mixture of isopropanol, DI water, and particle stock at 4:5:1 volumetric ratio. Before experiments, the spreading solution was sonicated for at least 10 minutes at room temperature. To get the syringe as close as possible to the interface, the syringe was attached to a custom-made 3D printed syringe holder that sits on the Langmuir trough and holds the syringe at 45°. The syringe holder secured syringes at a fixed height from the interface such that the attached needle was directly above the interface's desired location. Before adding the oil supraphase, an unfilled syringe was used to

extract excess water/glycerol subphase to set the interface height. Oil was then added. Finally, a syringe filled with spreading solution and particles was placed in the syringe holder, allowing the particles to be placed directly at the interface.

The double wall ring geometry was attached to the rheometer and located to the interface using axial force measurements in TRIOS (TA Instruments) software. Oil was then added to the system. To ensure particles would cover the whole interface, the geometry was moved down into the water phase during particle injection to the interface. Using the syringe holder the spreading solution was injected at the interface at 3 locations. After particles are added to the interface, interfaces were allowed to reach equilibrium microstructures over 3 hours and 30 minutes.

The surface coverage of the particles for every experiment varied and was controlled via volume of particle solution added and particle concentration in the solution. Actual measured surface concentrations are shown in Table 1. Across a single nominal surface concentration, the bidisperse particle systems are generally within uncertainty of each other and close to the nominal value. Both monodisperse interfaces have slightly lower surface concentrations then intended typically.

| $\Gamma_{calc}$ | A100 | A70C30 | A50C50 | A30C70 | C100 |
|---|---|---|---|---|---|
| 50% | 47±15 | 53±10 | 53±4 | 56±4 | 42±4 |
| 38% | 34±4 | 46±2 | 39±2 | 42±3 | 30±3 |
| 27% | 23±8 | 35±3 | 25±3 | 35±3 | 15±2 |

Table 1: Intended surface concentrations as calculated by volume added compared to measured surface concentration from actual surfaces. Values are average surface concentration across three positions on the interface and uncertainty is the standard deviation of those measurements.

*Interfacial Rheology and Imaging*

A Discovery HR-20 equipped with a double wall ring was used to measure interfacial storage and loss moduli using small amplitude oscillatory shear.[53] Amplitude sweeps were conducted with strain rates from 0.002% to 20% at a frequency of 1 rad/s and the response of the interface was recorded. Interfacial measurements can be impacted by bulk flow, checked by the Boussinesq Number

$$Bo = \frac{Force_{surface}}{Force_{bulk}} = \frac{G^*_{surface}\gamma_{surface}P_i}{G^*_{bulk}\gamma_{bulk}A_s} = \frac{G^*_{surface}}{G^*_{bulk}H} \quad (1)$$

where $G^*_{surface}$ represents the surface complex modulus, $G^*_{surbulkface}$the bulk complex modulus, γ the applied strain, $P_i$ the probe's contact perimeter, $A_s$ the probes surface area of contact, and H a representative length scale derived from $P_i/A_s$. *Bo* values from low to moderate indicate considerable torque due to bulk flows and low sensitivity: double wall rings generate high Bo values because $P_i/A_s$ = 0.7 $mm^{-1}$. Considering the subphase system's viscosity of 2 mPa*s, $P_i/A_s$, and the observed range of surface moduli (0.00001 to 0.01 Pa·m), *Bo* values typically range between approximately 7 and 7000. The reported interfacial moduli have been further adjusted to cancel bulk effects, using a correction code provided by Dr. Jan Vermant.[53] A minimum detectable moduli, $10^{-5}$ Pa*m, was calculated based on the rheometer's minimum torque.[54]

A custom designed trough was used that enabled both control of the surface concentration via a Langmuir trough, and interfacial visualization, which has been outline previously.[55] A Mitutoyo Lense M plan Apo 50X / 0.55 f=200 long distance and a IL-5S camera (Fastec, 1280 × 1024 pixels, 5 μm pixel) at 500 fps

were used to capture images interfaces. Images of stable microstructures at each interface across three locations were taken prior to testing.

Images were auto adjusted for brightness and contrast, followed by automatic thresholding in ImageJ. Black and white thresholded images were used to find fractal dimensions via box-counting and surface concentration using ImageJ. Changing automated in brightness, contrast, and thresholding routines and values were evaluated and found to not significantly alter fractal dimensions or surface concentrations derived.

## Results

*Impact of bidispersity on microstructure*

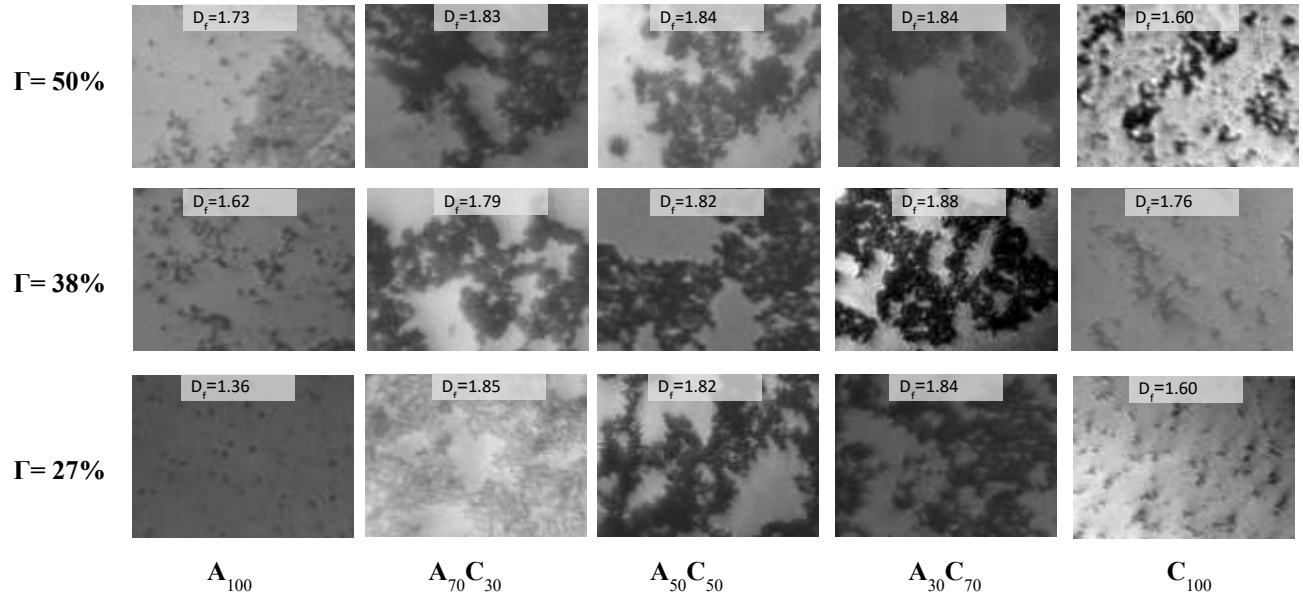


**Figure 1:** Microstructures of Amidine and Carboxylate mixtures at o/w with 0.05M salt concentration in the subphase. Each image is annotated with a fractal dimension, $D_f$, which were calculated from images at 3 locations. Average values are reported. Across all systems the standard deviation was exceedingly small, average value of .02, which is treated as the uncertainty for these measurements. 1280 × 1024, 5 μm pixels, 500 fps and a 50X Mitutoyo lens. Auto brightness/ contrast adjustment in ImageJ were done on all images.

At the lowest surface concentration, small, isolated clusters of particles were observed for the monodisperse amidine system (Figure 1). These clusters qualitatively grew in size and complexity of shape with increasing surface concentration. Increasing complexity was measured directly via fractal dimension, which for the amidine system increased from 1.36 to 1.73 with increasing surface concentration. Pure carboxylate behaved similarly, but shape complexity was not impacted with increasing surface concentration. Pure system images had particles out of the focal plane, creating a blurrier effect in comparison to the bidisperse systems. This was consistent with the lower surface concentrations measured in Table 1.

As was initially observed in the work of Nallaimilli and coworkers looking at charge bidisperse interfaces,[41] bidisperse populations of particles increased interface microstructure complexity. Qualitatively, this is observed as the more network like structures of the bidisperse interfaces. This is

quantitatively confirmed through examining the fractal dimensions of the interfaces. For all the bidisperse systems, the fractal dimensions are larger than the monodisperse and range from 1.79 to 1.85. Changes in fractal dimensions did not appear to have any specific trend with the changes in relative concentration of amidine/carboxylate particles or surface concentrations. For most systems, the values of fractal dimensions for the three tested bidisperse interfaces were nearly identical. The most dramatic difference between the monodisperse and bidisperse interfaces in fractal dimension is observed at the lowest surface concentration.

In some images, we see small regions of darker particles within rafts/structures particularly in the A100 50% surface concentration interface. These could be an indication of the formation of small multi-layer regions within the larger monolayer. Alternatively, they are also possibly due to inconsistent lighting and/or particle variability.

*Impact of Bidispersity on Interfacial Rheology*

In previous work with bidisperse hydrophobic/hydrophilic interfaces, increase in system elasticity was observed as relative concentrations between particles reached equi-fraction and all systems had higher moduli when bidisperse in comparison to monodisperse results.[51] Charge bidisperse systems also had larger moduli than corresponding monodisperse systems across most surface fractions tested at 0.05M NaCl.

The impact of charge bidispersity was least significant at the highest surface concentration evaluated, 50%. Examining the results, the A100, A70C30, and A50C50 interfaces all had nearly identical storage and loss moduli and were dominated by their elastic response (Figure 2). The A30C70 interface had slightly lower moduli than all these systems. A30C70 had a measurable modulus that was also dominated by elasticity, whereas the pure carboxylate system was below system resolution. Based on Table 1, these systems all had surface concentrations within error of each so they can be treated as equivalent.

For $\Gamma$= 38%, both sets of monodisperse interfaces are very weak and nearly below the resolution of the rheometers. However, all bidisperse systems provide a measurable interface. In fact, all three bidisperse interfaces for this surface concentration exhibit moduli higher than the monodisperse systems. The bidisperse A70C30 system is clearly the strongest system with moduli ~ 1.5 orders of magnitude larger than A50C50 and A30C70 system. Although the A70C30 system also has the largest surface concentration (Table 1), the variations in surface concentrations are less than 10% which does not create changes in moduli as large as observed.[32] The A50C50 and A30C70 have similar moduli to each other, but are no longer elastic dominated, and the pure systems are essentially below measurement range.

At 27% surface concentration, all systems are viscous dominated, and moduli are quite small; it is difficult to draw any conclusions.

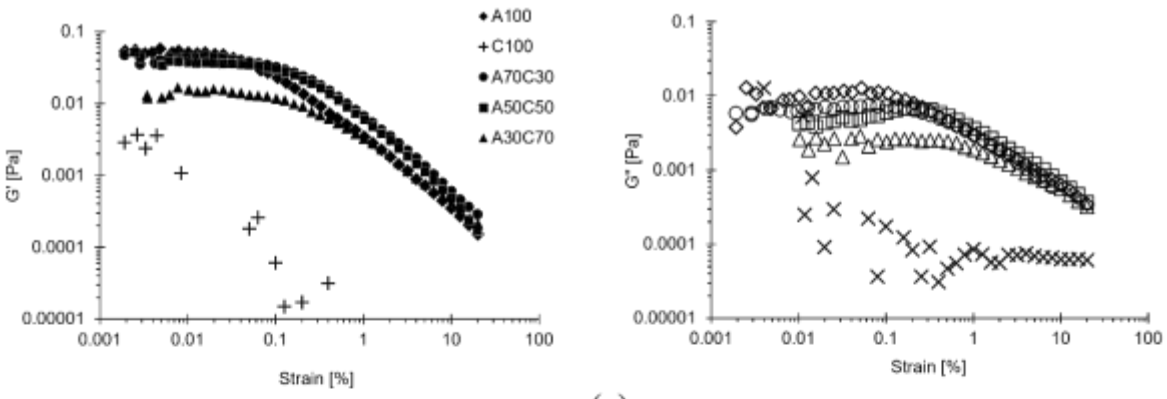


(a)

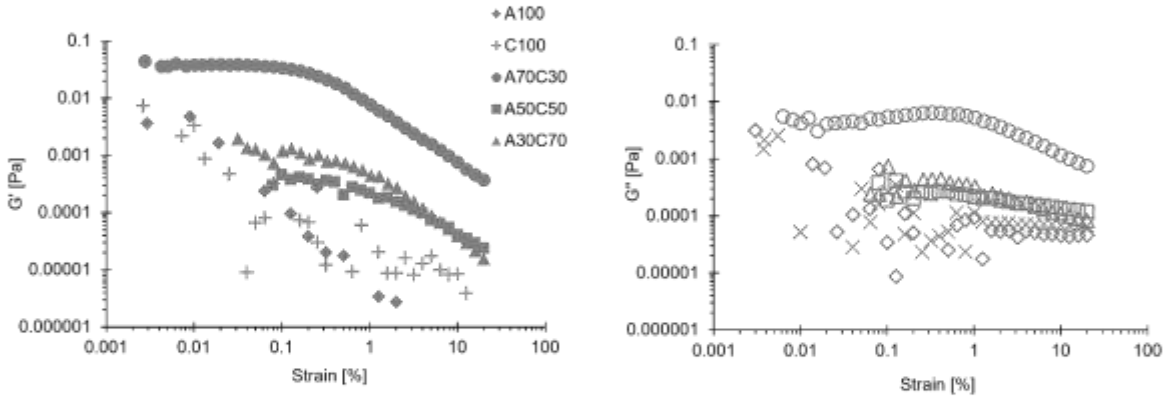


(b)

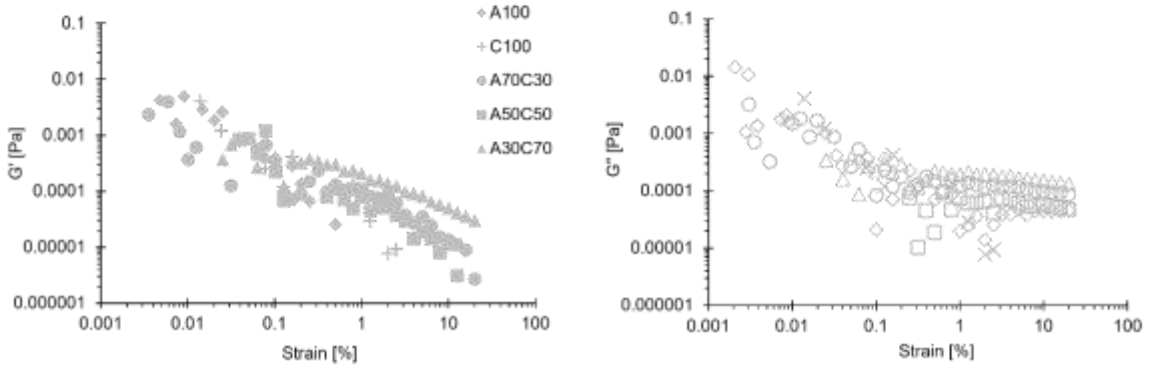


(c)

**Figure 2:** (a) Γ =50%, (b) Γ =38%, and (c) Γ =27% storage and loss moduli for AXXCYY subjected to strain rates ranging from 0.002% to 20% at 1 rad/s and at a salt concentration of 0.05M. Storage moduli on the left and loss on the right.

*Nature of Dipole*

The force due to the electrostatic dipole can be carried through either the polar or non-polar phase of the fluid as mentioned previously. This may cause fundamental changes to both the strength of the dipole, as well as the length scale of the interaction. To determine how the electrostatic dipole force behaved in this system, salt concentration in the polar DI water/Glycerol subphase was altered over several orders of magnitude. Changes in salt concentration impact the Debye length in the polar phase, and therefore would impact the dipolar force if it acts, even only partially through the polar subphase. Figure 3 shows how a bidisperse system, A70C30, at the o/w interfaces behaves with changing salt concentration.

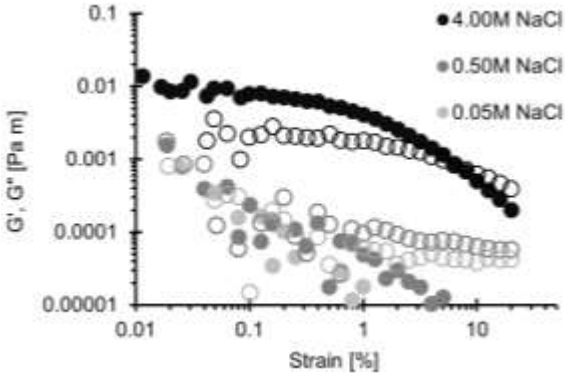


**Figure 3:** Effect of Increasing Salt Molarity in the Subphase on the Viscosity of the Interface of the oil water interface at Γ = 27% and A70C30 and strain rate of 0.002% to 20%.

As molarity of the salt increases, so does the storage moduli up to the maximum salt concentration of 4M NaCl concentration. 4M NaCl represents the uppermost limit of salt solubility in our subphase. The results indicate that the electrostatic dipole force is transmitted through the polar phase and the dipole is occurring at least partially through particle/polar charge screening.

*Impact of bidispersity on yield stress*

The goal of this work is to implement increased stability in emulsions with lower surface coverage than typically used. The results show that using bidispersity may be a way to achieve this for higher salt, lower surface concentration systems. For the 50% surface concentration, the monodisperse amidine and the amidine majority systems all exhibited similar results (Figure 2 and 4), indicating at moderate surface concentration bidispersity had less impact. The weakest interface was the A30C70 (Figure 4). These variations appear to be due to bidispersity, given the surface concentrations are all equivalent based on variability. At these surface concentrations, the decrease of hydrophobic attraction by reducing the amidine particles appeared to be balanced by the increase electrostatic attraction between carboxylate and amidine particles.

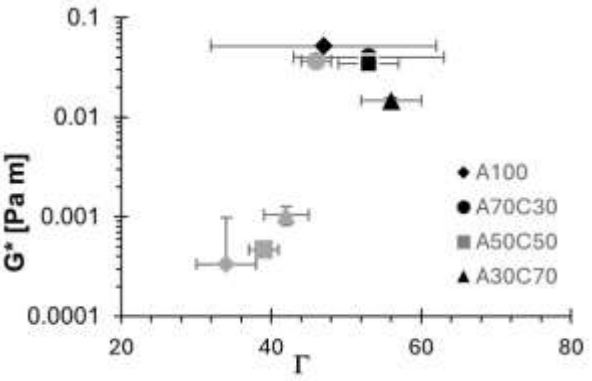


**Figure 4:** Linear complex moduli, G*, vs. actual surface concentration for 0.05 NaCl. C100 and 27% data not shown because it of low values. Error bars represent standard deviation. Y error bars in some cases are hidden by symbol. Dark symbols are the nominal 50% interfaces and gray the nominal 38% interfaces.

As 38% surface concentration, the bidisperse systems were stiffer than pure systems (Figure 2 and 4), particularly the A70C30 system. The A100 system is the lowest surface concentration measured. A30C70 is slightly stronger then the A50C50. The reason for this is unclear. As mentioned previously, this was not likely due to variations in surface concentrations;[32] as can be seen in Figure 4, these systems were all relatively close in actual surface concentration when variation is considered. In general, the increased

electrostatic attraction due to carboxylate particles is effective at increasing surface moduli for this surface concentration, despite the reduction in hydrophobic interaction.

At 27% surface concentration, it is difficult to draw any specific conclusions about the role of bidispersity.

Changing salt concentration, based on Figure 3 and table 2, impacted the relative effectiveness of bidispersity, making the bidisperse systems stiffer, which seems counterintuitive given the reduction in electrostatic attraction.

| Salt Concentration | A70C30 |
|---|---|
| 0.05M | N/A |
| 0.50M | N/A |
| 4.00M | $4.0 \times 10^{-4}$ |

**Table 2:** Yield stress of A70C30 interfaces at an oil water interface with the presence of different NaCl concentrations in the subphase. Units in Pa*m

Previous work,[18] found interfacial yield stress to be the means of stabilizing gas bubbles with values of ~$10^{-4}$ Pa M needed. It is unclear if such values are sufficient for emulsions. Interfacial yield stresses of studied systems were estimated by the yield strain multiplied by the linear storage modulus and are shown in Table 2 and 3. For those systems with measurable moduli, Table 3 shows that moduli reach the benchmark value for all 50% interfaces except the pure carboxylate. Interestingly, despite the moduli being similar, the yield stress of the bidisperse interfaces were larger than the pure amidine, suggesting that the interfaces although similar in overall strength have varying behavior in yield. Changes in this value indicate the impact of microstructure.[35] As salt increases, the benchmark yield stress value is also reached (Table 2).The results of this work indicate that the enhancement of interfacial moduli through bidispersity is possible and may be able to yield sufficient moduli/yield stress for stabilization.

| Γ | A100 | A70C30 | A50C50 | A30C70 | C100 |
|---|---|---|---|---|---|
| 50% | $1.8 \times 10^{-4}$ | $6.5 \times 10^{-4}$ | $5.9 \times 10^{-4}$ | $2.6 \times 10^{-4}$ | N/A |
| 38% | N/A | $7.7 \times 10^{-4}$ | $3.2 \times 10^{-5}$ | $6.8 \times 10^{-5}$ | N/A |
| 27% | N/A | N/A | N/A | N/A | N/A |

**Table 3:** Yield stress of different systems at the oil water interface with the presence of 0.05M NaCl in the subphase. Units in Pa*m.

*Modeling composition specific interfacial viscoelasticity*

Examining the charge bidiperse systems at o/w interfaces in this work, differences with the previous work are immediately noticeable. Charge bidisperse interfaces were more networked/complex compared to monodisperse systems, consistent with previous work on bidisperse charged systems[41] and mixed wettability systems.[51] However, the increased complexity did not depend on the overall surface concentration and/or the relative surface fraction of the particles like the previous studies. Negatively charged particles of bidisperse wettability at a/w interfaces exhibit increased interfacial moduli as relative particle fractions reach 50/50 at all surface concentrations.[51] Charge bidisperse systems exhibit increased moduli inconsistently at o/w interface: bidispersity had an essentially neutral impact for 50% surfaces in terms of moduli magnitude. Furthermore, they reached maximum moduli at a 70/30 split of particles.

Observed enhancement of moduli and changes in microstructure due to bidispersity clearly depends on system specific composition parameters, including overall surface concentration, relative surface concentration, type of bidispersity, and subphase composition. To implement bidisperse systems intelligently, the impact on interfacial moduli must be predictable. Previously, it was hypothesized that the increased interfacial moduli with bidisperse particle systems was due in part to increasing complexity/network microstructure.[51] In that work, changes in elasticity correspond to increased microstructure complexity as observed by fractal dimension. However, elasticity increases also correspond with a relative force asymmetry metric. Neither microstructure nor force asymmetry could fully capture the observed moduli increase.

Both microstructure and moduli depend on the interparticle forces; the differences between previous work and current work therefore must be due to changes in the underlying system composition impacting those forces. To model the impact of bidispersity and predict at what relative particle fraction maximum moduli occur, the net force in the system is considered, which is based on examinations of moduli variation in monodisperse systems.[35] The overall force on a system, $F_{net}$, can be estimated based on the average force per particle, $\langle F \rangle$, and the total number of particles,

$$F_{net} = \frac{A_i \Gamma}{\pi r^2} \langle F \rangle \tag{2}$$

where $A_i$ is the interfacial area, the area of the particle is assumed to be equivalent to its largest cross section, and are particles are assumed to be the same nominal radius. The average force per particle can be estimated by the probability of interactions between various particles,

$$\langle F \rangle = P_{aa}F_{aa} + P_{ab}F_{ab} + P_{bb}F_{bb} \tag{3}$$

$$P_{aa} = \%_a \%_a;\ P_{bb} = \%_b \%_{b;}\ P_{ab} = 2\%_a \%_b \tag{4}$$

$$\langle F \rangle = \%_a^2 (F_{aa} + F_{bb} - 2F_{ab}) + 2\%_a (F_{ab} - F_{bb}) + F_{bb} \tag{5}$$

where $P_{iy}$ is the probability of interaction between any two particles, and % is the relative percentage of each particle on the interface. The percentage of one type of particle where the maximum moduli occur should correspond to the maximum of the $<F>$,

$$\frac{d\langle F \rangle}{d\%_a} = 0 \ \rightarrow \%_{a,Max\ Modulus} = \frac{F_{bb} - F_{ab}}{F_{aa} + F_{bb} - 2F_{ab}} \tag{6}$$

Using equation (6), it should be possible to find a system specific relative surface fraction that creates the strongest interface; however, it does require that the interparticle interactions are known or calculable. This is not altogether trivial. As previously mentioned, there are two primary forces to act on all particles, plus hydrophobic attraction.

To calculate the net force and/or its maximum requires calculation of the forces between the particles, $F$. As mentioned previously, there are several interactions that can be considered.

The magnitude of the capillary attraction between particles is based primarily on particle radius, contact line undulation magnitude, and the capillary multipole type. Assuming a capillary quadrupole, the in-line force takes the form,[24]

$$F_{cap} = -48\pi\gamma h_i h_j \cos 2\left(\varphi_i - \varphi_j\right)\frac{(r_i r)^2}{{L_{ij}}^5} \quad (7)$$

where $\gamma$ is surface tension, $h$ is the magnitude of contact line undulation, $\varphi$ is the quadrupole angle, $L$ is the center-to-center distance between the particles, and $r$ is the particle radius. Although this cannot be assumed for all systems, for this work it is reasonable to assume that all particles have the same undulation magnitude and size given the similar synthesis and composition. Therefore, the magnitude of the capillary forces for aligned quadrupoles will be the same between *a* and *b, a* and *a*, and *b* and *b* particles. This results in capillary forces having no impact on equation (6) and but does impact equation (5).

Given the results of examining salt concentration, each particle is modeled as having electrostatic dipole forces due to the electric field created by the charges at the particle/polar phase interface, which can be modeled as,[22]

$$F_{el} = \frac{3\varepsilon_n}{2\pi\varepsilon_0\varepsilon_w^2}\frac{p_a p_b}{L^4} \ (L \gg r) \quad (8)$$

Where $p$ represents the dipole magnitude of an individual particle, $L$ is the separation between the particles, and $\varepsilon_n$ is the dielectric constant of the non-polar phase, $\varepsilon_w$ is the dielectric constant of water, and $\varepsilon_o$ is permittivity of free space. The dipoles are then,

$$p = \frac{q}{\kappa} \quad (9)$$

where $\kappa^{-1}$ is the Debye length of the particle and $q$ is equivalent point charge at the waters interface, which is,

$$q = \sigma_c * 2\pi R^2(1 + \cos\theta) \quad (9)$$

where $\sigma_c$ is the colloidal surface charge density and $\theta$ is the contact angle of the particle.[20]

The Debye length of each was calculated from ionic concentration.[56] contact angles for both amidine (100°)[41] and carboxylate (70°)[57] were found in literature. The average separation between particles is not known, but given many particles are in close contact *L=2r,* is assumed for all calculations. For the purposes of modeling, $h$ is assumed to be on the order of 10nm[24] and the particles were assumed to be in perfect alignment.

The charge density used in equation (9) is difficult to know apriori, since the actual charge will be changed by the solvent qualities (salt and ph)[58] and the degree of disassociation and manufacture.[59] There are some theoretical models for the surface charge at the interface,[20] and they can be measured via fitting of those models to surface pressure isotherms.[60-61] A thorough study on carboxylate particles in solution found surface charges on the order of -1 μc/cm$^2$ to -20 μc/cm$^2$ for salt concentrations ranging from 1 mM to 1000mM at a range of ph's. For latex particles of unknown surface functionalization, surface charges at an octane/water interface where found to be anywhere from 1%[61] ~ 35%[62] of the manufacturer value. Given the wide potential range of values and potential difference between materials, the surface charge provided by the manufacture or measured was used in models to be consistent; impacts of changes to surface charge will be discussed below.

Van der wals forces, which should be attractive between like particles and may be attractive or repulsive between dissimilar particles, could also be considered due to the close packed nature of the particles. Fundamentally, this force is mediated by the interface, and in the most simplistic take, an effective Hamaker constant which is based on area fraction of the particle in each phase can be used to calculate this force.[63-65] When particles are at close range on interfaces, it has been found that the this force scales with $1/L$,[64-65] which when used to estimate with typical Hamaker constants was found to be several orders of magnitude less than both capillary and dipole forces. Furthermore, in a variety of studies, capillary attraction has been found to be the dominant attractive mechanism experimentally,[35] in simulations,[38-39] and when used to theoretical predict interfacial elasticity.[23]

Finally, the hydrophobic attraction will only exist in between hydrophobic particles. Unfortunately, there is no convenient theoretical form for this force. It could be used as a free fitting parameter. However, using data from Figure 3, the value can be estimated by assuming systems with similar $F_{net}$ should create similar moduli. Using equation (2) and equating $F_{net,1} = F_{net,2}$,

$$F_H = \frac{\langle F\rangle_{2-F_h} - \frac{\Gamma_1}{\Gamma_2}\langle F\rangle_{1-F_h}}{\frac{\Gamma_1}{\Gamma_2}\%_{a,1}^2 - \%_{a,2}^2} \tag{10}$$

assuming particle $a$ is the hydrophobic particle.

This is only an estimate of the hydrophobic force, and it makes several assumptions about the nature of the force: it is unaffected by total number of particles on the interface and the relative ratio of particles. From Figure 2, several systems with similar moduli in the linear regime are observed which could be used to calculate a value of $F_H$: Γ = 50% A100C0, A70C30, A50C50 and Γ=38% A70C30. Using the 50% systems, $F_H$ is calculated to have a value of -5.2±0.4 x$10^{-12}$ N, which is similar in value to the forces calculated for $F_{el}$. If the lower surface concentration system is used to calculate, a larger value results, indicating that the assumptions mentioned above regarding the constancy of the hydrophobic force are not entirely valid.

Using the calculated value, $F_{net}$ is plotted as a function of relative surface fraction of amidine for the amidine/carboxylate systems in Figure 4. Without the hydrophobic force, the minimum curve occurs at 36%, but with the hydrophobic force, the relative prediction for the maximum is moved to a relative fraction of amidine of 85%. This seems to correspond well with the value for the 50%. Furthermore, based on Figure 5, for the 50% interface the equivalence between the A100, A70C30, and A50C50 in Figures 2 is

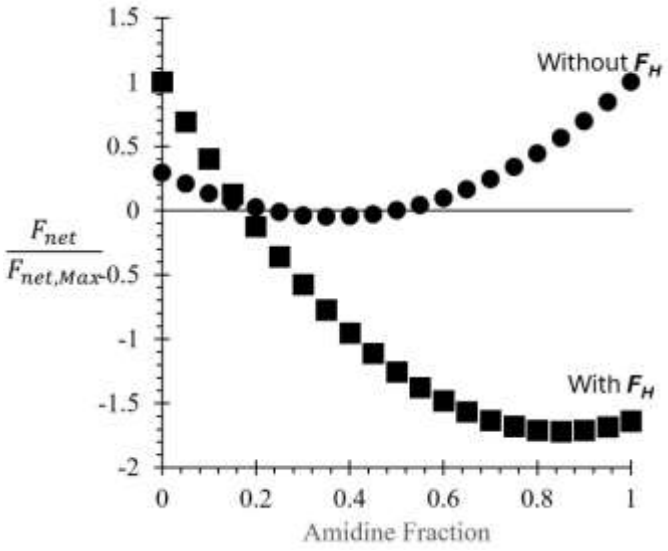


**Figure 5:** $F_{net}$ as predicted by equation (5) for Amidine/Carboxylate interfaces. $F_{net}$ is presented non-dimensionally by the maximum net dipolar force from that curve.

reasonable. Furthermore, the A30C70 and C100 having the weakest interface is predicted. The model does seem to accurately match the interface as measured.

The 38% interface matches the predicted maximum in Figure 5. It exhibits A100 and A50C50, as having similar moduli (Figure ?) which is consistent with Figure 5. However, A30C70 is seen to be stronger than those 2 interfaces, which is not consistent with prediction. These errors may be due to changes in the surface concentration

In general, modulus increase with bidispersity relies on changes to the Net force, and the attractive force asymmetry sets the relative fraction where max moduli occur.

It should be possible to predict relative surface fraction with maximum moduli using Equation (6) if details of the system composition are known and the forces can be modeled/estimated as above. Using the same hydrophobic amidine particles and sulfate particles (contact angle 70°)[57] the net force as a function relative amidine fraction is shown in Figure 5 for a 50% surface concentration system.

The predicted point of maximum moduli is an amidine fraction of 100% (Figure 6, left). Both amidine compositions should have measurable moduli with increasing strength towards increasing amidine concentration. Pure sulfate should be a very weak interface based on these predictions. The experiment corresponds well to the predictions. The pure system has larger moduli than the bidisperse, as before. But the A70S30 has a large modulus and the A30S70 has measurable but much weaker.

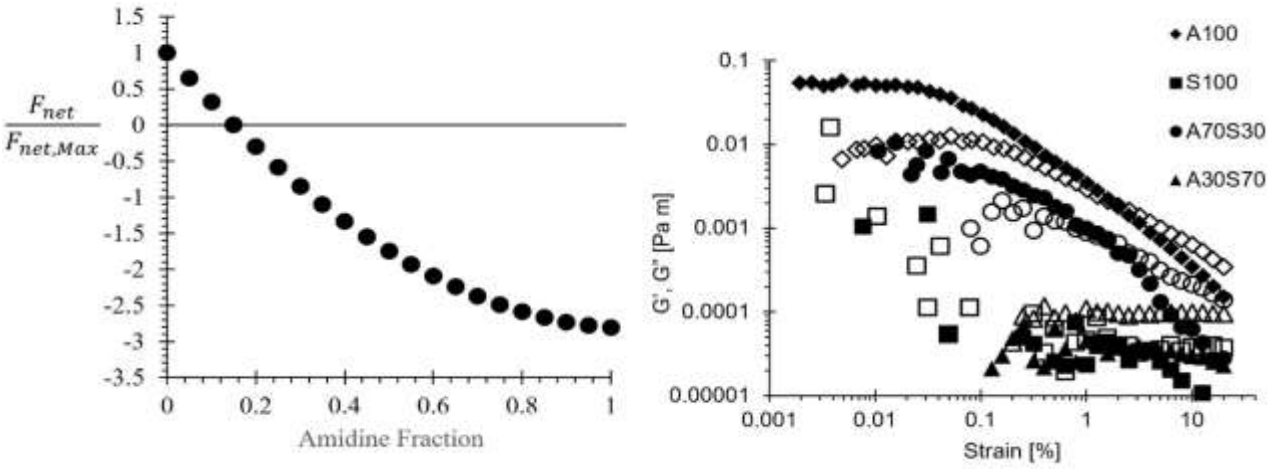


**Figure 6:** (Left) $F_{net}$ as predicted by equation (5) to find the amidine fraction which should correspond to maximum modulus. (Right) Experimental measured Moduli for Amidine/Sulfate systems. 0.05 M NaCl 50% surface concentration.

*Model accuracy and utility*

The net force modeled appears to capture the general trends of bidispersity of charge well for the location of the interface with maximum modulus. It cannot predict changes in relative elasticity, which have been observed for hydrophobic/hydrophilic bidisperse systems.[51] These would appear to be impacted by

microstructure and the nature of the forces themselves. However, given the general nature of the model, it can theoretically predict the behavior of other systems and/or be used to decouple the effects of wettability and charge on interfaces. However, there are several caveats in its application and use that must be addressed.

As described above, the model used manufacturer surface charges, which are a high estimate. Reducing those charges by considering the actual surface charge in water would change the predictions. In fact, reducing the charge of the negative particle further pushes maximum towards greater amidine fraction, as can be seen for the sulfate system which has lower surface charge than the carboxylate based on manufacturer specifications. Assuming some differential charge disassociation based on particle type, a change to the location of the maximum modulus is expected, which might better correlate to experimental results.

Lowering surface charges of both particles to values more than an order of magnitude lower than the ones used, as might be predicted by dissociation, decreases the dipole force, increasing the impact of the capillary/hydrophobic forces. When these systems are modeled, a parabolic curve with the minimum beyond 1 is predicted, indicating that the maximum modulus resides at the hydrophobic particle fraction being 100%. A similar result can be implemented by artificially increasing the hydrophobic force.

Based on the results shown in Figure 2 and 4, the surface charges and hydrophobic force calculation somewhat accurately represent the 50% and 38% surface concentration data. Issues in individual predictions compared to data, may be due to variation in surface concentration. Alternatively, the dominance of the pure amidine in the 50% surface concentration system may be due to the surface charge used in the prediction or the hydrophobic force being wrong. It is impossible to know which of these is occurring, since hydrophobic force is calculated using the dipole force which relies on surface charge. The very small value of the moduli for the pure amidine system in the 38% surface concentration may be due to overprediction of the hydrophobic force, since it the 50% surface concentration interfaces were used to find this value or changes in the surface charge as well. Again, it is impossible to know which of these is occurring, since hydrophobic force is calculated using the dipole force which relies on surface charge.

The relative balance of the various forces is paramount to the model's success. Correct estimation of forces is needed to accurately use the proposed model and expand it to other systems, and accurate calibration of the hydrophobic force constant is essential. Given this, accurate application of the model to other systems requires a reasonable estimate of the hydrophobic force which may only be possible via experimentation.

## Conclusion

Results from this work show that interfacial moduli can be increased via bidispersity consistent with the initial hypothesis. Specifically, it was found that interfacial moduli could be increased by 1 order of magnitude and yield stresses could be created at surface concentrations below 50% when using bidisperse interfaces compared to monodisperse interfaces. These improvements may enable emulsion stabilization.[18] Microstructural analysis shows that mixed systems form more complicated, networked structures compared to pure systems, which is consistent with previous work examining microstructure of bidisperse particle systems at o/w interfaces.[41, 51] This structural complexity is linked to changes in trends/behavior of the viscoelastic moduli and the moduli magnitude to increases in overall attraction

between particles on the interface, which is consistent with observations of higher surface concentration systems.[32, 37]

The system with maximum moduli is not tied to 50/50 relative fraction of particles, but at the system composition that maximizes overall attraction between particles on the interface. The surface concentration where moduli are maximum can be predicted by evaluating the net force in the system using the model proposed in this work, which corresponded well with experimental observations. This model only has a single fitting parameter, which in some instances can be calculated/calibrated via experiments. This new model improves upon the previous attempts to collapse data,[51] and importantly shows that moduli are increased by increasing overall magnitude of attractive forces between particles. In this work, this was done via bidisperse changes to system composition increasing electrostatic interactions; however, the model suggests that any system composition changes that increase overall attraction would create similar effects. Therefore, the model has the potential impact to predict a range of other bidisperse conditions (such as wettability, size, shape…).

Our findings improve the understanding of system composition impacts interparticle forces and how those influence the viscoelastic properties of particles at oil/water interfaces. Using the model, changes to system composition should be able to predictably engineer stronger o/w interfaces under appropriate system compositions when a full cataloging of the forces acting between particles is made. Using the results, future studies of more complicated systems where changes in forces are made through both particle composition and also sub/supra phase composition will be undertaken to explore if similar adjustments to interfacial yield stress can be created in a predictable way.

**Acknowledgements**

The authors would like to acknowledge NSF CBET Grant #2127637 for funding of this work.

**Author Contributions**

AA conducted all experimental work and aided in data analysis, writing, and editing. GFC aided in experimental design, data analysis, writing, and editing.

**Reference**


1. Lee, J.; Babadagli, T., Optimal design of pickering emulsions for heavy-oil recovery improvement. *J. Dispersion Sci. Technol.* **2020,** *41* (13), 2048-2062.
2. Wang, Y.; Sun, B.; Hao, Z.; Zhang, J., Advances in Organic–Inorganic Hybrid Latex Particles via In Situ Emulsion Polymerization. *Polymers* **2023,** *15* (14), 2995.
3. Ribeiro, A.; Lopes, J. C. B.; Dias, M. M.; Barreiro, M. F., Pickering Emulsions Based in Inorganic Solid Particles: From Product Development to Food Applications. *Molecules* **2023,** *28* (6), 2504.
4. Linke, C.; Drusch, S., Pickering emulsions in foods-opportunities and limitations. *Crit. Rev. Food Sci. Nutr.* **2018,** *58* (12), 1971-1985.
5. Cheon, J.; Haji, F.; Baek, J.; Wang, Q.; Tam, K. C., Pickering emulsions for functional food systems. *J. Agric. Food Res.* **2023**, 100510.
6. Zheng, Z.; Zhao, Y.; Ye, Z.; Hu, J.; Wang, H., Electrically conductive porous MXene-polymer composites with ultralow percolation threshold via Pickering high internal phase emulsion templating strategy. *J. Colloid Interface Sci.* **2022,** *618*, 290-299.
7. Ma, T.; Cui, R.; Lu, S.; Hu, X.; Xu, B.; Song, Y.; Hu, X., High internal phase Pickering emulsions stabilized by cellulose nanocrystals for 3D printing. *Food Hydrocolloids* **2022,** *125*, 107418.
8. Zhao, X.; He, F.; Yu, G.; Feng, Y.; Li, J., High-viscosity Pickering emulsion stabilized by amphiphilic alginate/SiO2 via multiscale methodology for crude oil-spill remediation. *Carbohydr. Polym.* **2021,** *273*, 118492.
9. Zhou, Y.; Sun, S.; Bei, W.; Zahi, M. R.; Yuan, Q.; Liang, H., Preparation and antimicrobial activity of oregano essential oil Pickering emulsion stabilized by cellulose nanocrystals. *Int. J. Biol. Macromol.* **2018,** *112*, 7-13.
10. Guzmán, E.; Ortega, F.; Rubio, R. G., Pickering Emulsions: A novel tool for cosmetic formulators. *Cosmet.* **2022,** *9* (4), 68.
11. Ramsden, W., Separation of solids in the surface-layers of solutions and 'suspensions'(observations on surface-membranes, bubbles, emulsions, and mechanical coagulation).—Preliminary account. *Proc. R. Soc. London* **1904,** *72* (477-486), 156-164.
12. Wu, J.; Ma, G. H., Recent studies of Pickering emulsions: particles make the difference. *Small* **2016,** *12* (34), 4633-4648.
13. Correia, E. L.; Razavi, S., Janus particle amphiphilicity and capillary interactions at a fluid interface. *AIChE J.* **2023**, e18241.
14. Sarkar, A.; Dickinson, E., Sustainable food-grade Pickering emulsions stabilized by plant-based particles. *Curr. Opin. Colloid Interface Sci.* **2020,** *49*, 69-81.
15. Griffith, C.; Daigle, H., Destabilizing Pickering emulsions using fumed silica particles with different wettabilities. *J. Colloid Interface Sci.* **2019,** *547*, 117-126.
16. Yang, Y.; Fang, Z.; Chen, X.; Zhang, W.; Xie, Y.; Chen, Y.; Liu, Z.; Yuan, W., An overview of Pickering emulsions: solid-particle materials, classification, morphology, and applications. *Front. Pharmacol.* **2017,** *8*, 235054.
17. Pitois, O.; Rouyer, F., Rheology of particulate rafts, films, and foams. *Curr. Opin. Colloid Interface Sci.* **2019,** *43*, 125-137.
18. Beltramo, P. J.; Gupta, M.; Alicke, A.; Liascukiene, I.; Gunes, D. Z.; Baroud, C. N.; Vermant, J., Arresting dissolution by interfacial rheology design. *PNAS* **2017,** *114* (39), 10373-10378.
19. Bayles, A. V.; Vermant, J., Divide, conquer, and stabilize: Engineering strong fluid–fluid interfaces. *Langmuir* **2022,** *38* (21), 6499-6505.
20. Oettel, M.; Dietrich, S., Colloidal Interactions at Fluid Interfaces. *Langmuir* **2008,** *24* (4), 1425-1441.

21. Guzmán, E.; Ortega, F.; Rubio, R. G., Forces controlling the assembly of particles at fluid interfaces. *Langmuir* **2022,** *38* (44), 13313-13321.
22. Park, B. J.; Pantina, J. P.; Furst, E. M.; Oettel, M.; Reynaert, S.; Vermant, J., Direct Measurements of the Effects of Salt and Surfactant on Interaction Forces between Colloidal Particles at Water−Oil Interfaces. *Langmuir* **2008,** *24* (5), 1686-1694.
23. Danov, K. D.; Kralchevsky, P. A.; Naydenov, B. N.; Brenn, G., Interactions between particles with an undulated contact line at a fluid interface: Capillary multipoles of arbitrary order. *J. Colloid Interface Sci.* **2005,** *287* (1), 121-134.
24. Kralchevsky, P. A.; Denkov, N. D.; Danov, K. D., Particles with an undulated contact line at a fluid interface: interaction between capillary quadrupoles and rheology of particulate monolayers. *Langmuir* **2001,** *17* (24), 7694-7705.
25. Danov, K. D.; Kralchevsky, P. A., Capillary forces between particles at a liquid interface: general theoretical approach and interactions between capillary multipoles. *Adv. Colloid Interface Sci.* **2010,** *154* (1-2), 91-103.
26. Botto, L.; Lewandowski, E. P.; Cavallaro, M.; Stebe, K. J., Capillary interactions between anisotropic particles. *Soft Matter* **2012,** *8* (39), 9957-9971.
27. Rahman, M. A.; Beltramo, P. J., Rough colloids at fluid interfaces: From fundamental science to applications. *Front. Phys.* **2023,** *11*, 1248706.
28. Weijgertze, H. M.; Kegel, W. K.; Zanini, M., Patchy rough colloids as Pickering stabilizers. *Soft Matter* **2020,** *16* (34), 8002-8012.
29. Wouters, M.; Aouane, O.; Sega, M.; Harting, J., Capillary interactions between soft capsules protruding through thin fluid films. *Soft matter* **2020,** *16* (48), 10910-10920.
30. Petkov, P. V.; Danov, K. D.; Kralchevsky, P. A., Monolayers of charged particles in a Langmuir trough: Could particle aggregation increase the surface pressure? *J. Colloid Interface Sci.* **2016,** *462*, 223-234.
31. Cappelli, S.; de Jong, A. M.; Baudry, J.; Prins, M. W., Interparticle capillary forces at a fluid–fluid interface with strong polymer-induced aging. *Langmuir* **2017,** *33* (3), 696-705.
32. Rahman, S. E.; Laal-Dehghani, N.; Barman, S.; Christopher, G. F., Modifying interfacial interparticle forces to alter microstructure and viscoelasticity of densely packed particle laden interfaces. *Journal of colloid and interface science* **2019,** *536*, 30-41.
33. Tabor, R. F.; Grieser, F.; Dagastine, R. R.; Chan, D. Y., The hydrophobic force: measurements and methods. *PCCP* **2014,** *16* (34), 18065-18075.
34. Bergfreund, J.; Bertsch, P.; Fischer, P., Effect of the hydrophobic phase on interfacial phenomena of surfactants, proteins, and particles at fluid interfaces. *Curr. Opin. Colloid Interface Sci.* **2021,** *56*, 101509.
35. Barman, S.; Christopher, G. F., Role of capillarity and microstructure on interfacial viscoelasticity of particle laden interfaces. *J. Rheol.* **2016,** *60* (1), 35-45.
36. Moncho-Jordá, A.; Martınez-López, F.; Hidalgo-Alvarez, R., The effect of the salt concentration and counterion valence on the aggregation of latex particles at the air/water interface. *J. Colloid Interface Sci.* **2002,** *249* (2), 405-411.
37. Reynaert, S.; Moldenaers, P.; Vermant, J., Interfacial rheology of stable and weakly aggregated two-dimensional suspensions. *PCCP* **2007,** *9* (48), 6463-6475.
38. Laal-Dehghani, N.; Christopher, G. F., 2D Stokesian Simulation of Particle Aggregation at Quiescent Air/Oil-Water Interfaces. *J. Colloid Interface Sci.* **2019**.
39. Laal-Dehghani, N.; Christopher, G. F., Effects of Interfacial Shear on Particle Aggregation at an Oil/Water Interface. *Langmuir* **2022,** *38* (31), 9621-9630.

40. Thakur, S.; Razavi, S., Particle Size and Rheology of Silica Particle Networks at the Air–Water Interface. *Nanomaterials* **2023,** *13* (14), 2114.
41. Nallamilli, T.; Ragothaman, S.; Basavaraj, M. G., Self assembly of oppositely charged latex particles at oil-water interface. *J. Colloid Interface Sci.* **2017,** *486*, 325-336.
42. Wilson, H. J.; Davis, R. H., Shear stress of a monolayer of rough spheres. *J. Fluid Mech.* **2002,** *452*, 425-441.
43. San-Miguel, A.; Behrens, S. H., Influence of nanoscale particle roughness on the stability of pickering emulsions. *Langmuir* **2012,** *28* (33), 12038-12043.
44. Guzmán, E.; Maestro, A., Soft Colloidal Particles at Fluid Interfaces. *Polymers* **2022,** *14* (6), 1133.
45. Zang, D.; Rio, E.; Delon, G.; Langevin, D.; Wei, B.; Binks, B., Influence of the contact angle of silica nanoparticles at the air–water interface on the mechanical properties of the layers composed of these particles. *Mol. Phys.* **2011,** *109* (7-10), 1057-1066.
46. Correia, E. L.; Brown, N.; Razavi, S., Janus Particles at Fluid Interfaces: Stability and Interfacial Rheology. *Nanomaterials* **2021,** *11* (2), 374.
47. Liu, L.; Ngai, T., Pickering Emulsions Stabilized by Binary Mixtures of Colloidal Particles: Synergies between Contrasting Properties. *Langmuir* **2022,** *38* (44), 13322-13329.
48. Qiao, Y.; Ma, X.; Liu, Z.; Manno, M. A.; Keim, N. C.; Cheng, X., Tuning the rheology and microstructure of particle-laden fluid interfaces with Janus particles. *Journal of Colloid and Interface Science* **2022,** *618*, 241-247.
49. Ballard, A. F.; Panter, J. R.; Wales, D. J., The energy landscapes of bidisperse particle assemblies on a sphere. *Soft Matter* **2021,** *17* (40), 9019-9027.
50. Monteux, C.; Jung, E.; Fuller, G. G., Mechanical Properties and Structure of Particle Coated Interfaces: Influence of Particle Size and Bidisperse 2D Suspensions. *Langmuir* **2007,** *23* (7), 3975-3980.
51. Rahman, S. E.; Laal-Dehghani, N.; Christopher, G. F., Interfacial viscoelasticity of self-assembled hydrophobic/hydrophilic particles at an air/water interface. *Langmuir* **2019,** *35* (40), 13116-13125.
52. Hiemenz, P. C.; Rajagopalan, R., *Principles of Colloid and Surface Chemistry, revised and expanded*. CRC press: 2016.
53. Vandebril, S.; Franck, A.; Fuller, G. G.; Moldenaers, P.; Vermant, J., A double wall-ring geometry for interfacial shear rheometry. *Rheol. Acta* **2010,** *49*, 131-144.
54. Zhang, Z.; Barman, S.; Christopher, G. F., Effect of interfacial viscoelasticity on the bulk linear viscoelastic moduli of globular protein solutions. *Phys. Rev. E* **2014,** *89* (5), 052306.
55. Barman, S.; Christopher, G. F., Simultaneous interfacial rheology and microstructure measurement of densely aggregated particle laden interfaces using a modified double wall ring interfacial rheometer. *Langmuir* **2014,** *30* (32), 9752-9760.
56. Russel, W. B.; Russel, W.; Saville, D. A.; Schowalter, W. R., *Colloidal dispersions*. Cambridge university press: 1991.
57. Maestro, A.; Guzmán, E.; Ortega, F.; Rubio, R. G., Contact angle of micro-and nanoparticles at fluid interfaces. *Curr. Opin. Colloid Interface Sci.* **2014,** *19* (4), 355-367.
58. Schulz, S.; Gisler, T.; Borkovec, M.; Sticher, H., Surface charge on functionalized latex spheres in aqueous colloidal suspensions. *J. Colloid Interface Sci.* **1994,** *164* (1), 88-98.
59. Martin-Rodriguez, A.; Cabrerizo-Vilchez, M.; Hidalgo-Alvarez, R., Surface characterization of latexes with different interfacial properties. *Colloids Surf., A* **1996,** *108* (2-3), 263-271.
60. Aveyard, R.; Clint, J. H.; Nees, D.; Paunov, V. N., Compression and structure of monolayers of charged latex particles at air/water and octane/water interfaces. *Langmuir* **2000,** *16* (4), 1969-1979.

61. Petkov, P. V.; Danov, K. D.; Kralchevsky, P. A., Surface pressure isotherm for a monolayer of charged colloidal particles at a water/nonpolar-fluid interface: experiment and theoretical model. *Langmuir* **2014,** *30* (10), 2768-2778.
62. Chen, W.; Tan, S.; Huang, Z.; Ng, T.-K.; Ford, W. T.; Tong, P., Measured long-ranged attractive interaction between charged polystyrene latex spheres at a water-air interface. *Phys. Rev. E: Stat. Nonlinear Soft Matter Phys.* **2006,** *74* (2), 021406.
63. Deshmukh, O. S.; van den Ende, D.; Stuart, M. C.; Mugele, F.; Duits, M. H., Hard and soft colloids at fluid interfaces: Adsorption, interactions, assembly & rheology. *Adv. Colloid Interface Sci.* **2015,** *222*, 215-227.
64. Bresme, F.; Oettel, M., Nanoparticles at fluid interfaces. *J. Phys.: Condensed Matter* **2007,** *19* (41), 413101.
65. Guzmán, E.; Abelenda-Núñez, I.; Maestro, A.; Ortega, F.; Santamaria, A.; Rubio, R. G., Particle-laden fluid/fluid interfaces: physico-chemical foundations. *J. Phys.: Condens. Matter* **2021,** *33* (33), 333001.

**TOC Graphical abstract**